

# Non-elastic responses of tall steel buildings subjected to across-wind forces

Yukio Tamura<sup>†</sup>

*Department of Architecture, Tokyo Institute Polytechnics  
1583, Iiyama, Atsugi, Kanagawa, 243-0297, Japan*

Hachinori Yasui<sup>‡</sup> and Hisao Marukawa<sup>‡‡</sup>

*Urban Environment Research Center, Izumi Sohken Engineering Co., Ltd.  
51 Minami-sode, Sodegaura, Chiba 299-0268, Japan*

**Abstract.** This paper presents an analytical method which takes into account the non-linearity of individual members, and discusses some case study results. It also discusses the relationship between member non-elastic behavior and excitation duration, and the relationship between member fracture and overall structure behavior. It is clearly demonstrated that the frame already shows almost unstable behavior due to long-columnization just before the occurrence of a column fracture. Then, a column fracture immediately induces a structural collapse mechanism.

**Key words:** across-wind force; non-elastic response; tall steel buildings; frame models; member cumulative ductility; member fracture; structural collapse mechanism.

---

## 1. Introduction

Wind loads, as well as seismic loads, are the critical lateral loads in design of tall buildings in Japan. Present wind resistant design criteria generally require mostly elastic behavior for buildings in Japan, because it has not been clarified how they would behave in the non-elastic region under extremely strong wind conditions.

Recently, research has been carried out into elasto-plastic response behavior during wind excitation and a forecasting technique (Tsujita *et al.* 1997). Furthermore, Ohkuma *et al.* (1997) have discussed the relation between power spectrum density of wind force and elasto-plastic energy, and proposed a response estimation method based on the application of energy balance to the wind resistant design of buildings. However, these studies were based on the lumped mass system with a single mass or several masses under the bi-linear hysteresis assumption for each story or for the overall structure. Therefore, they do not clarify non-elastic behavior of members and the relationship between story and member deformations, making it impossible to pursue the fracture process of the building in the ultimate state.

In order to achieve the performance based design adopted in the Building Standard Law of Japan

---

<sup>†</sup> Professor

<sup>‡</sup> Senior Research Engineer

<sup>‡‡</sup> Head

in 1998, the building performance around its ultimate limit state should be examined. This paper first describes an analytical method that takes into account the non-linearity of individual members. Second, it shows the relationship between member non-elastic behaviors and excitation duration in a time history response analysis. Third, it discusses the relationship between member fracture and overall structure behavior.

## 2. Analysis method

### 2.1. Member deformation and yielding condition

In the nonlinear analysis of a 2D frame employed in this study, the following are incorporated as the basic functions (Ogawa 1995). The analysis takes into account the geometrical non-linearity of individual members as well as the material non-linearity. The geometrical non-linearity includes the unstable behavior of the overall structure, such as long-columnization, buckling, etc., accompanied by beam sidesway. It also incorporates member shearing deflection as well as bending deflection.

A generalized hinge method is employed, which accounts for the axial force-bending moment yielding relationship in the end parts of members. The following equations are employed as the initial yield surface for box section members and wide flange members about their strong axes.

$$\frac{N}{N_y} \leq \alpha \quad F(M, N) = \left(1 - \frac{\alpha}{2}\right) \frac{M}{M_p} + \frac{1}{2\alpha} \left(\frac{N}{N_y}\right)^2 - \left(1 - \frac{\alpha}{2}\right) = 0 \quad (1)$$

$$\frac{N}{N_y} > \alpha \quad F(M, N) = \left(1 - \frac{\alpha}{2}\right) \frac{M}{M_p} + \frac{N}{N_y} - 1 = 0$$

where  $N$  is axial force,  $N_y$  is yield axial force,  $M$  is bending moment,  $M_p$  is full plastic moment,  $\alpha$  is  $A_w/A$ ,  $A$  is gross sectional area and  $A_w$  is web sectional area. Bi-linear hysteresis characteristics are assumed under uni-axial stress conditions.

Prager's kinematic hardening law is employed for the conditions of subsequent yield following primary yield. Under Prager's kinematic hardening law, the yield surface does not change in size or shape, but the center of the yield surface moves perpendicularly to the yield surface at the current stress point, as shown in Fig. 1.

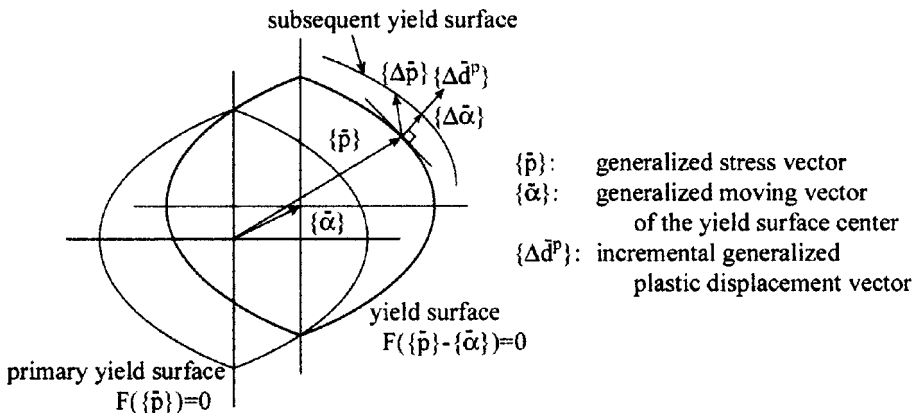


Fig. 1 Schematic of Prager's kinematic hardening law

## 2.2. Fracture conditions at member ends

The member end is assumed to fracture when its cumulative ductility ratio reaches 30, which is presumed to be appropriate according to experiments on steel members (JABRP 1998). The bending moment of the fractured end then becomes zero, forming a hinge.

## 2.3. Jointing panel behavior

The jointing panel is regarded as a shear panel having bi-linear hysteresis characteristics. The kinematic hardening law is also employed.

## 2.4. Frame models

Five 2D-frame models, A1, A2, A3, B1 and B2, as shown in Fig. 2, were analyzed. The building height of the Models A1, A2 and A3 is 300 m, and that of Models B1 and B2 is

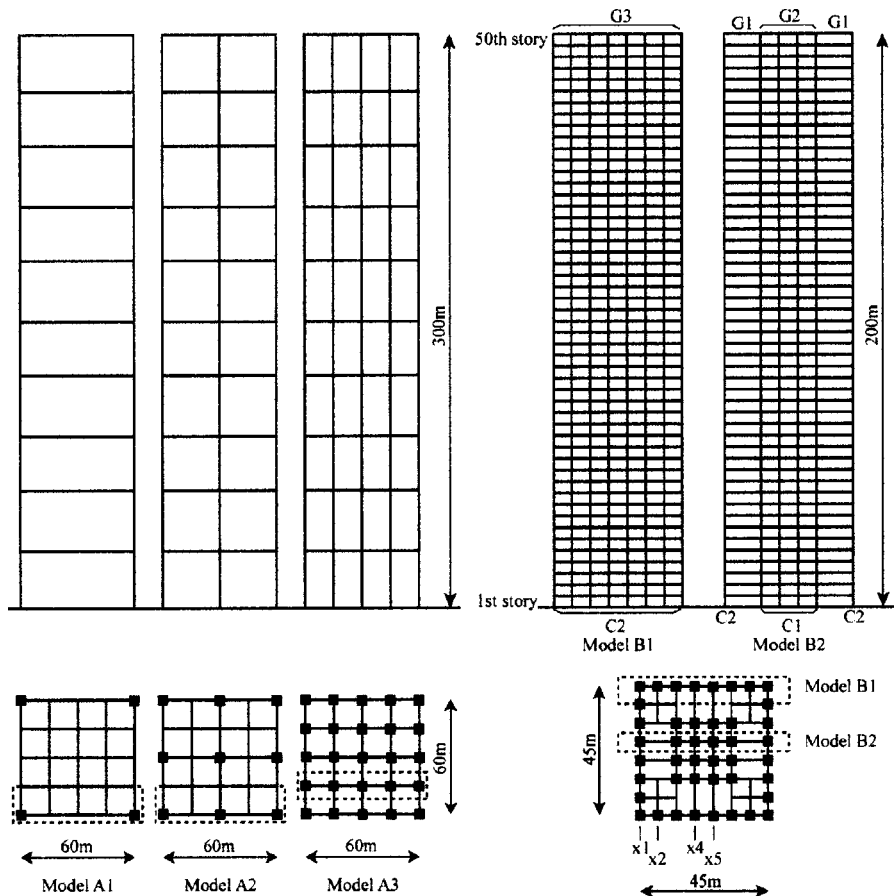


Fig. 2 Building models

Table 1 Column and beam section of Models A1, A2 and A3

Model	Story	Column	Beam	Model	Story	Column	Beam
A1	10	Box-1980x79	H-2491x996x50x66	A3	10	Box-1100x44	H-1405x562x28x38
	9	Box-2790x112	H-3989x1596x80x106		9	Box-1610x64	H-2129x852x43x57
	8	Box-3270x131	H-4963x1985x99x132		8	Box-1910x76	H-2560x1024x51x68
	7	Box-3640x146	H-5562x2225x111x148		7	Box-2120x85	H-2814x1126x56x75
	6	Box-3950x158	H-5981x2392x120x159		6	Box-2290x92	H-2986x1194x60x80
	5	Box-4240x170	H-6278x2511x126x167		5	Box-2430x97	H-3105x1242x62x73
	4	Box-4510x180	H-6480x2592x130x173		4	Box-2540x102	H-3191x1276x64x85
	3	Box-4800x192	H-6597x2639x132x176		3	Box-2630x105	H-3250x1300x65x87
	2	Box-5180x207	H-6583x2633x132x176		2	Box-2720x109	H-3283x1313x66x88
	1	Box-6280x251	H-5357x2143x107x143		1	Box-3060x122	H-3092x1237x62x83
A2	10	Box-1590x64	H-1952x781x39x52	Steel grade: SM490			
	9	Box-2290x92	H-3062x1225x61x82				
	8	Box-2680x107	H-3751x1500x75x100				
	7	Box-2950x118	H-4172x1669x83x111				
	6	Box-3150x126	H-4468x1787x89x119				
	5	Box-3310x132	H-4685x1874x94x125				
	4	Box-3430x137	H-4845x1938x97x129				
	3	Box-3520x141	H-4958x1983x99x132				
	2	Box-3660x146	H-5024x2010x101x134				
	1	Box-4290x172	H-4539x1816x91x121				

Table 2 Column and beam section of Model B1 and B2

Column (steel grade : SN490)			Beam (steel grade : SN490)		
Story	Index	Section	Story	Index	Section
36-50	C1, C2	Box-750x28	47-R	G1, G2, G3	H-750x250x12x22
31-35	C1	Box-750x40	37-46	G1, G2	H-750x300x14x22
	C2	Box-750x32		G3	H-750x250x14x22
26-30	C1	Box-800x40	32-36	G1, G2	H-750x300x14x25
	C2	Box-800x32		G3	H-750x250x14x25
11-25	C1	Box-800x45	17-31	G1, G2	H-750x350x14x25
	C2	Box-800x32		G3	H-750x300x14x25
1-10	C1	Box-800x70	2-16	G1	H-750x350x14x32
	C2	Box-800x55		G2	H-750x350x14x25
				G3	H-750x300x14x28

200 m. Models B1 and B2 are outside and inside frames of a structure, respectively. They consisted of square steel pipe columns and wide flange section beams, as shown in Tables 1 and 2.

The design conditions for these frames were as follows. Models A1, A2 and A3 were to be elastic for across-wind loads imposed by the 500-year recurrence wind speed (AIJ 1993), where the site was assumed to be in an open flat terrain and the 10-min-mean wind speed at the top  $V_H$  was

estimated at 73.3 m/s ( $H = 300$  m). Models A1, A2 and A3 are simplified and the number of their members were reduced so that many conditions could be analyzed and the basic characteristics of non-elastic response with member fracture could be clarified. Models B1 and B2 were designed to be maintained within the allowable stress range for the primary design earthquake load (AIJ 1993) and almost elastic for across-wind loads imposed by the 500-year recurrence wind speed (AIJ 1993), where the site was assumed to be in a city center and the mean wind speed  $V_H$  was estimated at 57.1 m/s ( $H = 200$  m). The base shear coefficient for the primary design earthquake was 0.067. The allowable stress was specified at the yielding stress, and the almost elastic limit as 1.1 times the yielding stress.

The frames were all designed to adopt a beam sidesway mechanism.

## 2.5. Preliminary study

Fig. 3 shows relation between relative story deformation angle and story shear force for Models A1, A2 and A3 under dead load and static wind load.

Fig. 4 shows the natural frequencies and modes of the models. Their fundamental mode frequencies were 0.15 Hz to 0.18 Hz. Since the design conditions of Model A-series were different from those of Model B-series, there was a difference between their vibration modes.

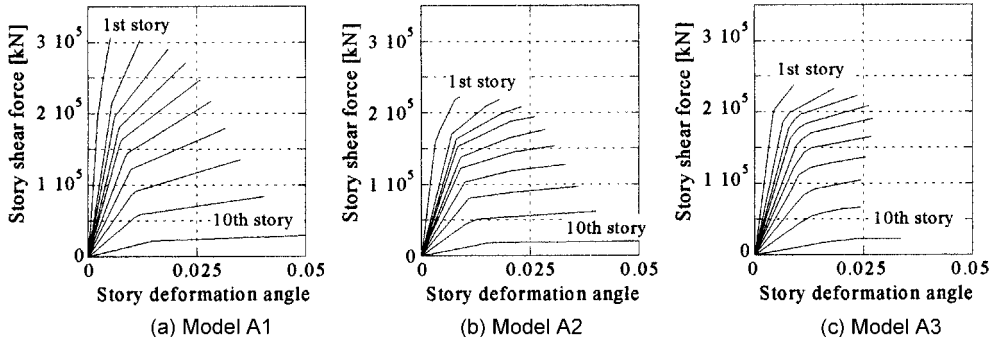


Fig. 3 Relation between story deformation angle and story shear force

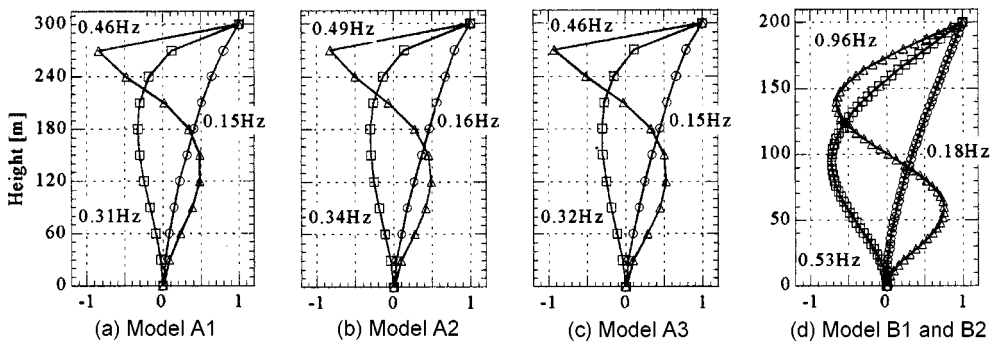


Fig. 4 Natural frequencies and modes of models

Table 3 Parameters for simulating wind forces

Parameters	Models A1, A2 and A3	Models B1 and B2
Site	Open flat terrain	City center
Mean wind speed at 10 m height	44.0 m/s: 500-year recurrence	26.9 m/s: 1000-year recurrence 28.5 m/s: 2000-year recurrence
Mean wind speed at the top	73.3 m/s: 500-year recurrence	60.4 m/s: 1000-year recurrence 64.0 m/s: 2000-year recurrence
Duration time	10 hours	10 hours
Time interval of wind force	0.25 s	0.25 s
Air density	1.25 kg/m <sup>3</sup>	1.25 kg/m <sup>3</sup>
Lag number of auto-correlation	500	1500

## 2.6. Response analysis

Time-domain wind-induced response analyses were made using Newmark's  $\beta$ -Method, where  $\beta$  was set at 1/4. The time interval for the numerical calculation was set at less than 1/100 of the natural period of the fundamental mode. The damping ratio (to the critical value) of the fundamental mode was set at 2% and the damping matrix was assumed to be proportional to the initial stiffness matrix. Dynamic wind forces were simulated using the method proposed by Tsukagoshi *et al.* (1993) and Tamura (1995) based on the auto-regression technique. Wind forces were generated for every story of building Models A1, A2 and A3, and for every two stories of building Models B1 and B2 (see Fig. 2 and Table 3). Static and dynamic external wind forces were applied after the dead load had been applied. Here, only the results for across-wind excitations are discussed, because the across-wind force is generally predominant in the wind resistant design of tall buildings.

## 3. Responses for cases without member fracture

### 3.1. Time history response

As the first step, the response analyses were made under the assumption that member fracture did not occur regardless of the value of its cumulative ductility factor.

Figs. 5a and 5b show temporal variations of strain energy and displacement of Model B1 subjected to across-wind excitation imposed by the 2000-year recurrence wind speed ( $V_H = 64.0$  m/s). As the frame was designed to adopt a beam sidesway mechanism, beam strain energy increases significantly and is shifted with beam member plasticity. The mean (moving average) displacements at the top of the model are shifted as well as the beam strain energy. However, column strain energy is almost constant and is equal to the dead load work on the columns.

Fig. 6 shows the temporal variations of energies and the level crossing number of Model A3 under across-wind excitation of 5000-year recurrence wind speed. The level crossing number is estimated every five minutes. Total energy, damping energy and strain energy increase with member plasticity, especially total energy and damping energy. The level crossing number varies slightly with member plasticity; however, no remarkable variation is found in the case without member fracture.

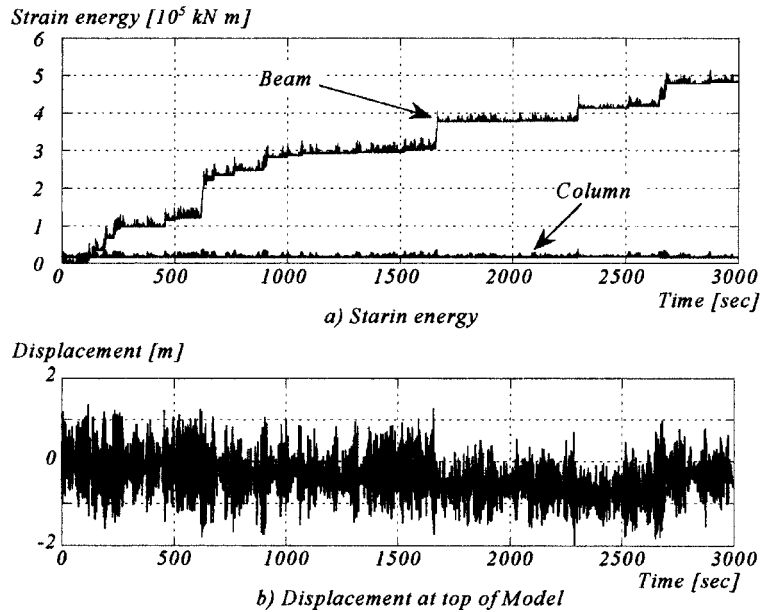


Fig. 5 Temporal variation of strain energies and displacement  
(Model B1, 2000-year recurrence, without member fracture)

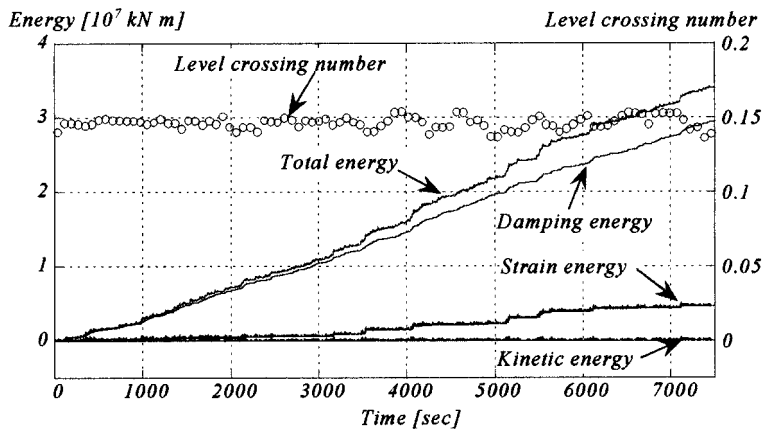


Fig. 6 Temporal variation of energies and level crossing number  
(Model A3, 5000-year recurrence, without member fracture)

### 3.2. Relation between story deformation and story shear force

Figs. 7a - 7c show the relation between excitation duration and story deformation and story shear force of the 8th story of Model B1 under across-wind excitation imposed by the 2000-year recurrence wind speed. The story deformation tends to move to the negative side with increment of excitation duration, and not back to the original point because of the  $P - \Delta$  effect. The  $P - \Delta$  effect also causes decrement of story shear force at yield point after 120 min as shown in Fig. 7c. A longer duration excitation causes more significant decrement of story shear force at yield point, which would induce

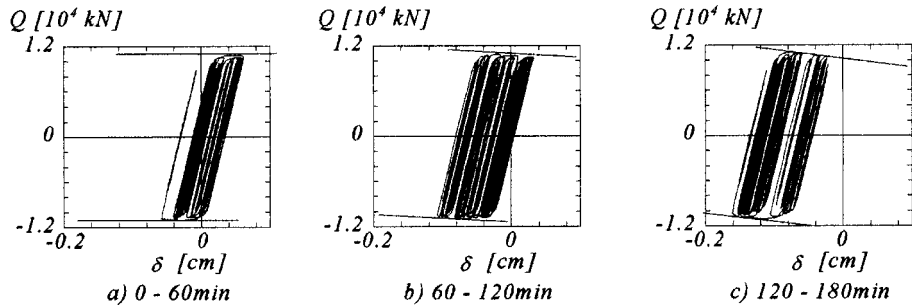


Fig. 7 Relation between excitation duration and story deformation and story shear force of the 8th story (Model B1, 2000-year recurrence, without member fracture)

structure collapse.

### 3.3. Excitation duration and plastic deformation of beams

A fluctuating wind speed simulation was conducted for 600 min and was divided into several samples. Response analyses were carried out 5 times for 120 min, 10 times for 60 min, 20 times for 30 min and 60 times for 10 min, for Models A1, A2 and A3.

Figs. 8a and 8b show the relations between the excitation duration and the ductility factors for a selected beam in the 5th story of Model A3 under across-wind excitations imposed by the 1000-year recurrence wind speed. The ordinate of Fig. 8a indicates the maximum value among the maximum ductility factors of the beam obtained for all samples for each excitation duration. The ordinate of Fig. 8b indicates the maximum value or mean value among the cumulative ductility factors for all samples for each duration time. No major difference is observed in the maximum values of the maximum ductility factors regardless of the excitation duration as shown in Fig. 8a. However, it is obvious that the mean and maximum cumulative ductility factors increase with excitation duration as shown in 8b, in particular, the mean cumulative ductility factor is almost proportional to the duration. This implies that the beam cumulative ductility factor for unit time is almost constant. The ductility factors for other beams on Model A1, A2 and A3 show the same tendency.

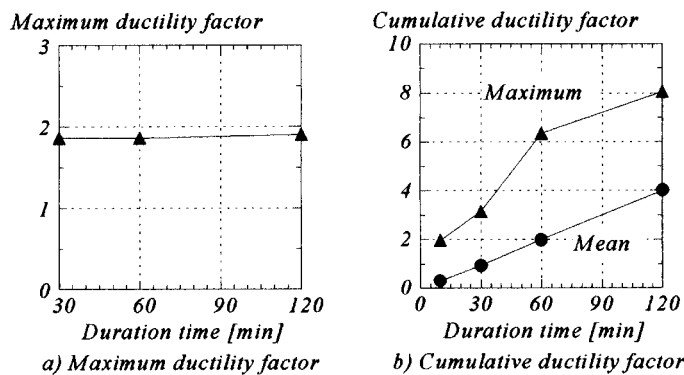


Fig. 8 Excitation duration and the maximum value of the maximum ductility factors and the cumulative ductility factor for a beam in the 5th story (Model A3, 1000-year recurrence, without member fractures)

If the beam sidesway mechanism and the same statistical wind force characteristics can be assumed, the above tendency may always be obtained. This tendency can be used to estimate cumulative ductility for a beam from that for a story. Since the relation between the relative story deformation and the beam end rotational deformation is obtained by a static frame model, it may be possible to roughly estimate cumulative ductility factor for a beam from the result based on the lumped mass system as follows :

- The cumulative ductility for the story  $CD_S$  can be obtained from the result based on the lumped mass system.
- Since cumulative ductility factor for unit time is almost constant, it is possible to assume that mean plastic deformation for unit time is constant. Therefore, mean plastic deformation  $\delta_u$  for unit time is obtained as:

$$\delta_u = \frac{CD_S}{T}$$

where  $T$  is the excitation duration.

- Assuming that the relation between relative story deformation and member deformation in dynamic analysis is almost the same in static analysis, the mean member deformation  $\theta_u$  for unit time is calculated from  $\delta_u$ .
- Then, the cumulative ductility factor for a beam  $CDF_E$  can be estimated as :

$$CDF_E = \frac{\theta_u T}{\theta_y}$$

where  $\theta_y$  means the member end rotational deformation at yield point.

### 3.4. Cumulative ductility factors of beams and story

Figs. 9a and 9b show the vertical distributions of the cumulative ductility factors of the beam ends for Models B1 and B2. The cumulative ductility factors reach maxima at 17th story for Model B1

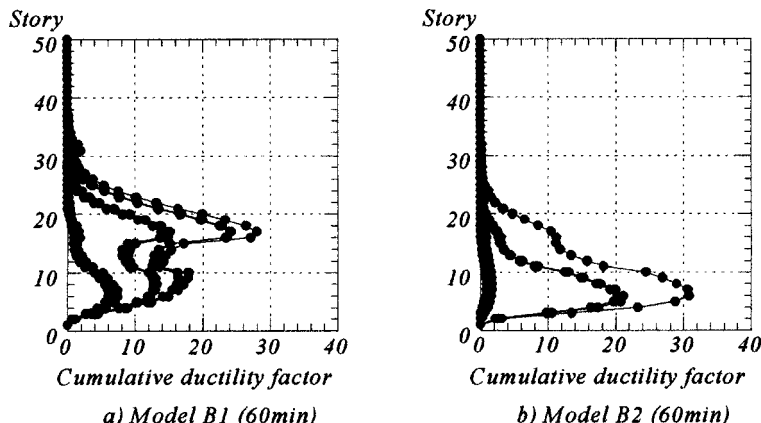


Fig. 9 Vertical distribution of the cumulative ductility factors  
(2000-year recurrence, without member fracture)

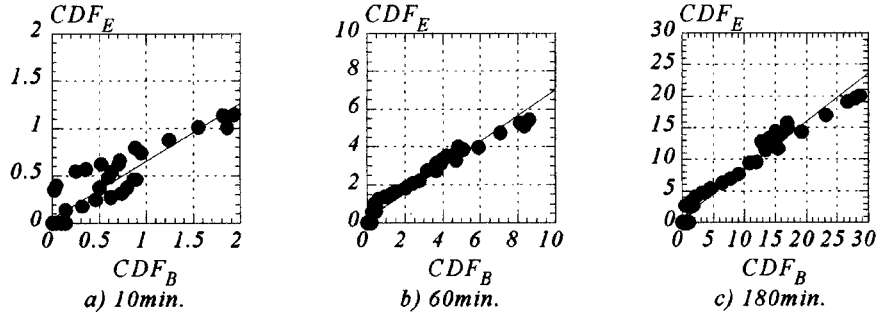


Fig. 10 Cumulative ductility factor for beams ( $CDF_B$ ) and those for stories ( $CDF_S$ ) based on frame model (Model B1, 1000-year recurrence, without member fracture)

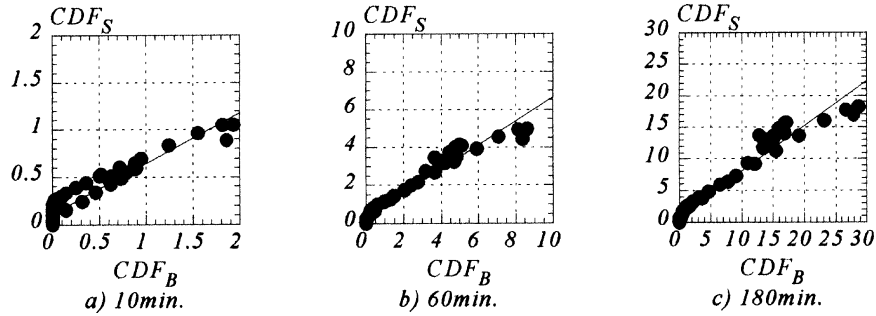


Fig. 11 Cumulative ductility factor for beams based on frame model ( $CDF_B$ ) and those on lumped mass system ( $CDF_E$ ) (Model B1, 1000-year recurrence, without member fracture)

and at 6th story for Model B2, and they increase with excitation duration.

Figs. 10a - 10c show the relation between cumulative ductility factor for beams ( $CDF_B$ ) and those for stories based on frame model ( $CDF_S$ ) under across-wind excitation.  $CDF_B$  is the maximum among all the beam ends of the story.  $CDF_S$  is the cumulative ductility factor calculated on the basis of story deformation and story shear force at which any one of the members in the story exceeded its yielding point.  $CDF_S$  are smaller than  $CDF_B$ .

Figs. 11a - 11c show relation between maximum beam cumulative ductility factor of the story based on the frame model ( $CDF_B$ ) and that estimated from the lumped mass system ( $CDF_E$ ) according to the above procedure.  $CDF_E$  are almost 25% ~ 30% smaller than  $CDF_B$ ; however, their agreement improves with increment of excitation duration. The difference occurs because a few beams become plastic for a short time.

No major difference was observed in the relation between  $CDF_E$  and  $CDF_B$  regardless of wind speed.

#### 4. Responses for cases with member fracture

##### 4.1. Progress of member end fractures

Figs. 12, 13a and 13b show the progress of member end fractures for Models A3, B1 and B2. The first fracture occurred at a beam end around the center span of the 7th story in Model A3, the 17th

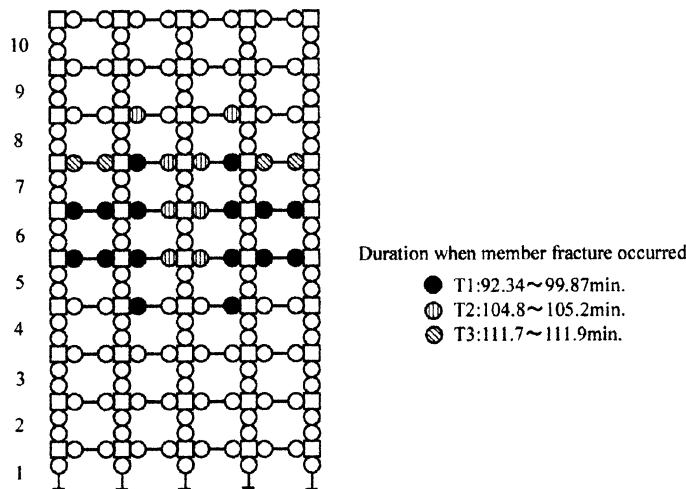


Fig. 12 Progress of member fractures of Model A3

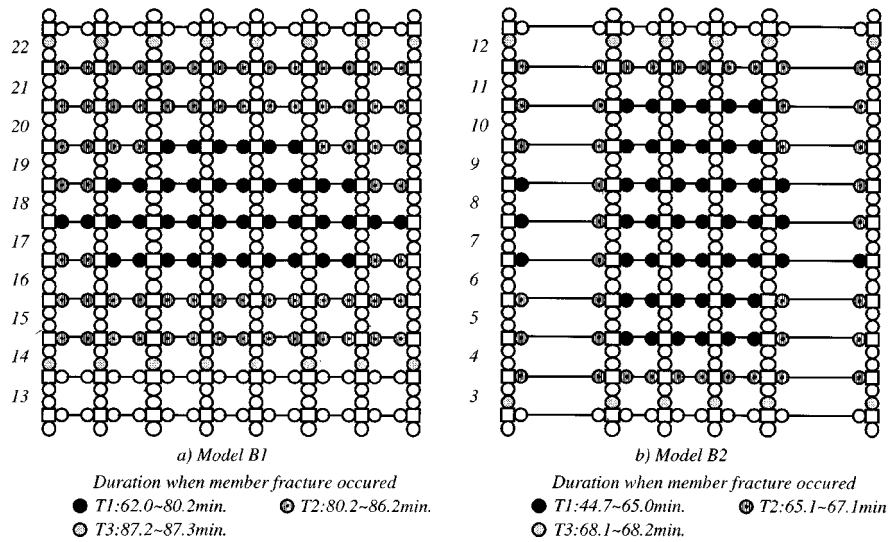


Fig. 13 Progress of member and fractures of Model B1 and B2 (2000-year recurrence)

story in Model B1 and 6th story in Model B2, and it propagated to the adjacent beam ends and the upper and lower stories. Neither model could resist external forces between stories, in which all column ends fracture, and they reach the collapse mechanism at duration  $T_3$ .

Analyses for change in wind force intensity were also carried out for Model A3. The layer at which column member fracture occurred differed or the collapse mechanism differed.

#### 4.2. Time history response

The temporal variation of story deformation angles, member bending moments and column axial forces on the 17th and 14th stories of Model B1 are shown in Figs. 14~17. A beam member end fracture occurred in the 17th story for the first time, and a column end fracture in the 14th story. In these figures,  $T1$  means the time that the first beam fracture occurred in the 17th story,  $T2$  means the time all the beams in each story fractured, and  $T3$  means the time the model reached the collapse mechanism. Also,  $t1$  means the time the second beam fracture occurred in the 17th story and  $t2$  means the time all the beams in the 14th story fractured.

As shown in Fig. 14, the fluctuation amplitudes of both deformation angles of the 17th story and 14th story increase with progress of beam end fractures, and their mean (moving average) values are shifted. In particular, that of the deformation angle of the 17th story, in which the first beam fracture occurred, increases drastically just after  $T2$ . Here, the increase in the natural period of the model is

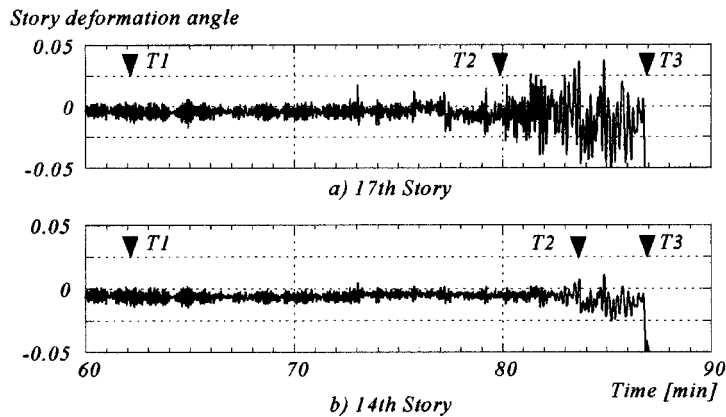


Fig. 14 Temporal variation of story deformation angles  
(Model B1, 2000-year recurrence)

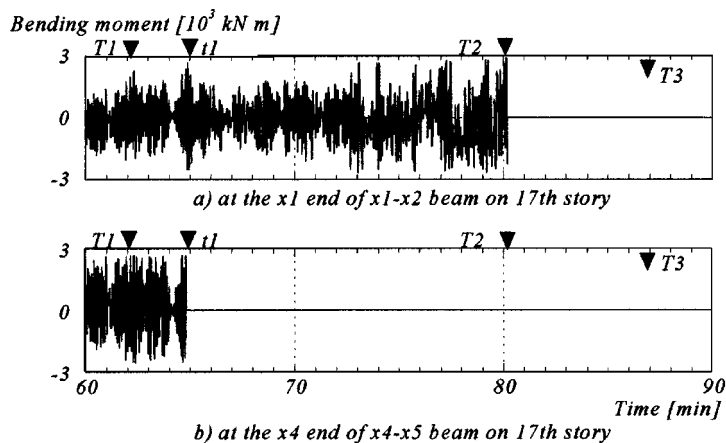


Fig. 15 Temporal variation of beam bending moment  
(Model B1, 2000-year recurrence)

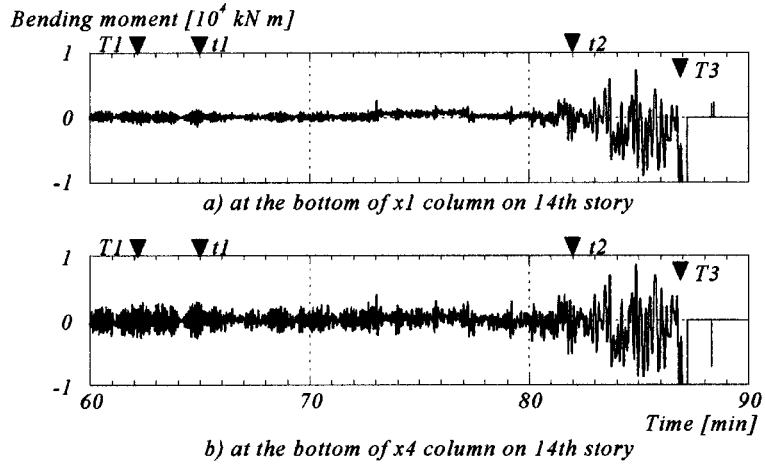


Fig. 16 Temporal variation of column bending moment  
(Model B1, 2000-year recurrence)

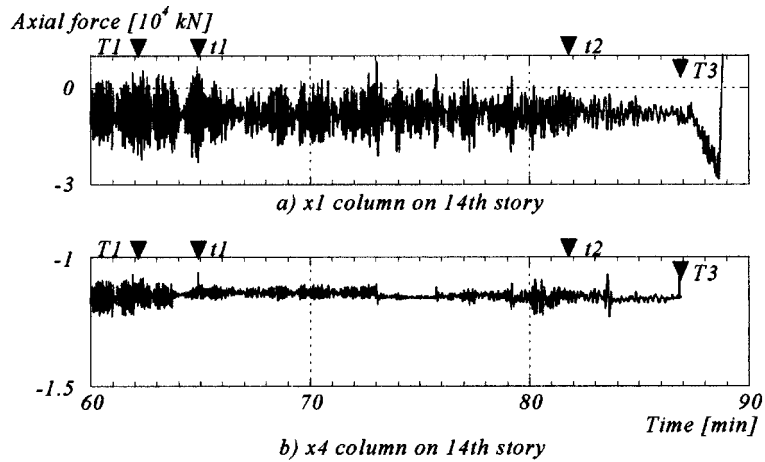


Fig. 17 Temporal variation of column member axial force  
(Model B1, 2000-year recurrence)

clearly observed after  $T_2$ .

Figs. 15a and 15b show bending moment fluctuations of the finally fractured beam end and the second fractured beam end of the 17th story. A fracture induces an instantaneous increment in member bending moments of the same story, but they immediately calm down with further propagation of the carry-over moment. The time lag between first beam fracture  $T_1$  and the last beam fracture  $T_2$  in the 17th story was greater than that in the 14th story, in which the column end fractures occurred, although the result is not shown here.

Figs. 16a and 16b show bending moments of an inside column  $x1$  and a corner column  $x4$  in the 14th story. The fluctuation amplitudes of the column bending moments increase drastically just after all the 14th story beams fracture ( $t_2$ ), and the frame soon reaches collapse mechanism just after all the 14th story beams fracture ( $t_2$ ), and the frame soon reaches collapse mechanism ( $T_3$ ). However,

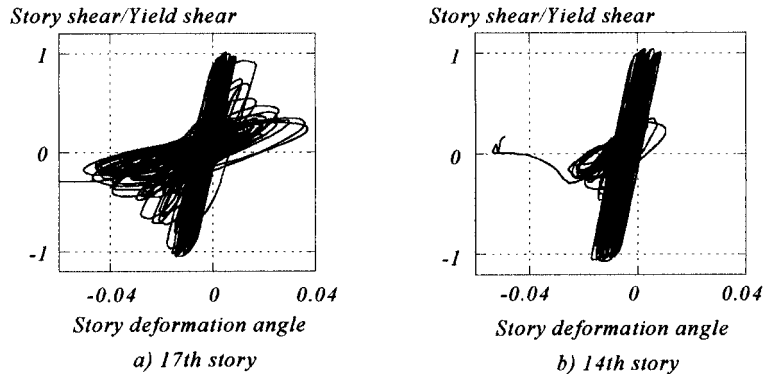


Fig. 18 Relation between story deformation angle and story shear force  
(Model B1, 2000-year recurrence, 0 min-87 min)

as shown in Figs. 17a and 17b, the amplitudes of their axial forces decrease after  $t_2$ , and become very small just before the collapse mechanism  $T_3$ . By precise observation of the Figs. 17a and 17b, some spiky instantaneous increments in the axial force amplitudes of the columns due to beam fractures are recognized. The axial force of the inside column  $x4$  shifts in a stepped manner at the same times.

#### 4.3. Story deformation and story shear force

Figs. 18a and 18b show the relation between story deformation angle and story shear force of the 17th and 14th stories. The slope of the hysteresis inclines with the member fractures. Thus, the stiffness decreases. This is quite different from the hysteresis for the case without member fractures shown in Figs. 7a ~ 7c. Therefore, the natural frequency of the model decreases as shown as temporal variation of the story deformation angle in Fig. 14.

#### 4.4. Phase-plane explanation

The building behavior around its collapse mechanism can be observed from the time histories of the story deformations or member stresses shown in Figs. 5~7 and 14~18. However, it is more clearly demonstrated by phase-plane explanation. Figs. 19a and 19b show the relation between the story deformation angle and the relative story velocity response for the 14th story of Model B1 without and with member fractures. As shown in Fig. 19a, for the case without member fractures, the orbit stays on the elliptic trace even when the member stresses exceed the elastic limit. However, as shown in Fig. 19b, for the case with member fractures, the orbit departed from the elliptic trace with significant increase in the story deformation angle just before the beginning of a column fracture. This might be induced by long-columnization. Immediately after the first column fracture, the relative story velocity increased its magnitude and reached the collapse mechanism of the building.

This suggests that the occurrence of plasticity in a column immediately results in a column fracture and collapse mechanism. Therefore, column plasticity or fracture should be avoided. According to the results of our study using the five frame models shown in Fig. 2, the beginning time of the column fracture was on average 1.8 times the beginning time of the beam fracture. If the beginning

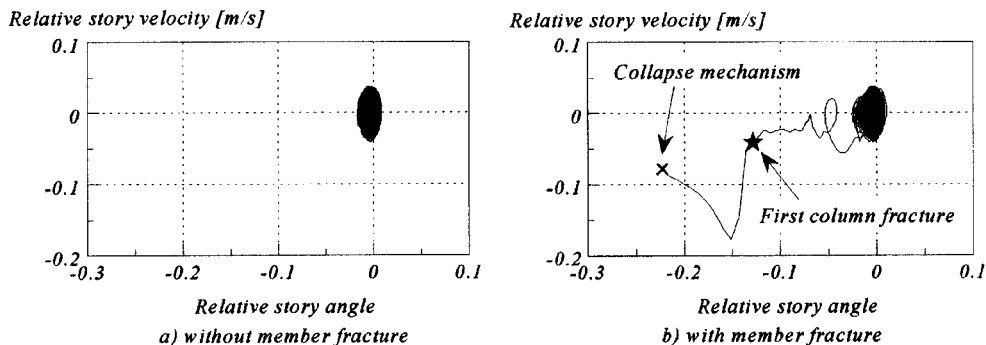


Fig. 19 Story deformation angle and relative story velocity response for 14th story  
(Model B1, 2000-year recurrence, 0 min-87.3 min)

time of the beam fracture can be estimated by the method shown in 3.3 using a lumped mass model, the collapse time can be roughly estimated.

## 5. Concluding remarks

The wind-induced non-elastic behaviors of building models have been examined, and the following points have been clarified. The level crossing number varies slightly with member plasticity, but no remarkable variation is found for the case without member fractures. However, the  $P\Delta$  effect causes decrement of story shear force at yield point. The cumulative ductility factor is proportional to the excitation duration.

Member fractures lower the natural frequency of the structure. Column bending moments increase drastically with beam end fracture. Just before the occurrence of a column fracture, the frame already shows almost unstable behavior due to long-columnization. Then, a column fracture immediately induces a structural collapse mechanism.

## Acknowledgements

The authors express sincere gratitude to Prof. K. Inoue of Kyoto University and K. Ogawa of Kumamoto University for their kind offer of non-elastic response analysis program for 2D frame models and useful discussions on the non-elastic behavior of steel buildings. They also thank Mr. T. Fukai for his assistance in the response analyses.

## References

- AIJ (1993), *Recommendation for Loads on Buildings*, Architectural Institute of Japan.
- JABRP (1998), *Recommendations on Loads for Performance Based Design*, Japan Association for Building Research Promotion. (in Japanese)
- Ogawa, K. (1995), *Research Report for Numerical Analysis*, Steel Material Club & Building Research Institute, Annex B. (in Japanese)
- Ohkuma, T., Kurita, T. and Ninomiya, M. (1997), "Response estimation based on energy balance for elasto-plastic vibration of tall building in across-wind direction", *Structural Safety and Reliability. Proceedings of ICOSSAR'97*, 1359-1366.

- Tamura, Y. (1995), "Numerical simulation program for structure response induced by wind loads - Technical Manual. *Tamura Laboratory*", Tokyo Institute of Polytechnics. (in Japanese)
- Tsujita, O., Hayabe, Y. and Ohkuma, T. (1997), "A study on wind-induced response for inelastic structure", *Structural Safety and Reliability. Proceedings of ICOSSAR'97*, 1359-1366.
- Tsukagoshi, H., Tamura, Y., Sasaki, A. and Kanai, H. (1993), "Response analyses on along-wind and across-wind vibrations of tall buildings in time domain", *Journal of Wind Engineering and Industrial Aerodynamics*, **46-47**, 497-506.